

# Assessing the Frontier: Active Learning, Model Accuracy, and Multi-objective Materials Discovery and Optimization

del Rosario, Zachary  
zdr@stanford.edu

Kim, Yoolhee  
ykim@citrine.io

Rupp, Matthias  
mrupp@citrine.io

Antono, Erin  
erin@citrine.io

Ling, Julia  
jling@citrine.io

December 23, 2021

## Abstract

Discovering novel materials can be greatly accelerated by iterative machine learning-informed proposal of candidates—active learning. However, standard *global-scope error* metrics for model quality are not predictive of discovery performance, and can be misleading. We introduce the notion of *Pareto shell-scope error* to help judge the suitability of a model for proposing material candidates. Further, through synthetic cases and a thermoelectric dataset, we probe the relation between acquisition function fidelity and active learning performance. Results suggest novel diagnostic tools, as well as new insights for acquisition function design.

## 1 Introduction

Accelerated design, optimization, and tuning of materials via machine learning is receiving increasing interest in science and industry. A major driver of this interest is the potential to reduce the substantial cost and effort involved in manual development, synthesis, and characterization of large numbers of candidate materials. The primary aim is to reduce the number of both failed candidates and development cycles.

A data-driven approach to achieve this acceleration is *active learning* (AL) [23], an iterative procedure in which a machine-learning model suggests candidate materials, a selection of which are synthesized, characterized, and fed back into the model to complete a learning iteration. The objective of this procedure varies; in materials informatics it is often to identify promising material candidates by optimizing properties of interest. Recent work has leveraged AL for materials when there is a *single objective* [1, 4, 6, 9, 12, 14, 16, 17, 21, 28–33, 37, 38]. However, new issues arise when optimizing multiple objectives simultaneously, as is frequently the case beyond proof-of-principle settings.

Furthermore, the aim to identify promising material candidates is distinct from the aim to improve model accuracy, a frequent objective in AL [22]. In fact, model accuracy can be at odds with acquiring optimal candidates: Figure 1 demonstrates that the usual global notion of model accuracy is not necessarily associated with optimal materials discovery. In this work, we introduce a notion of model accuracy more closely associated with rapidly discovering new materials.

We offer two primary contributions: First, we introduce new concepts to judge the performance of multi-objective AL, with an aim towards the specific concerns of materials discovery. In addition to the usual notion of multi-objective optimality [11]—non-dominance—we use criteria informed by the concept of *strata*—recursive non-dominance—from the database literature [19]. We also introduce *scoped* error metrics, which emphasize regions of interest in performance (property) space, particularly bands about the Pareto frontier we call *Pareto shells*. We demonstrate that the usual global-scope error provides less usable signal for candidate discovery performance, while Pareto shell error—under certain conditions—correctly signals when AL will likely identify performant candidates. Second, we compare multi-objective acquisition functions (also known as *improvement criteria*) in terms of their quantitative and qualitative performance. Specifically, we compare a collection of exploitation/exploration-navigating acquisition functions: Probability of Joint

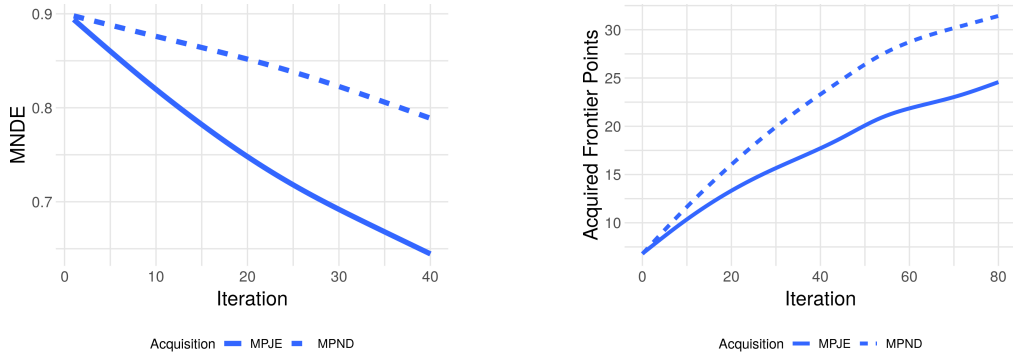


Figure 1: *Best global-scope error does not guarantee optimal candidate discovery.* Shown are global prediction errors (MNDE, left) and number of improved candidates found (right). The MPJE decision criterion (solid line) has lower errors, but leads to worse candidates than the MPND criterion (dashed line). Simulated active learning on a thermoelectric dataset. MNDE = Mean Non-Dimensional Error (7); MPJE = Maximum Probability of Joint Exceedance

Exceedance (PJE), Hyperplane Probability of Improvement (HPI), and Probability Non-Dominated (PND). These acquisition functions differ in terms of the fidelity with which they represent the Pareto frontier, allowing us to study how this affects AL performance.

In this work we review AL for single-objective materials discovery, review relevant concepts from multi-objective optimization, and synthesize materials-relevant concepts for judging AL performance. We introduce a family of acquisition functions (decision-making strategies), and compare their performance across several synthetic datasets and real a thermoelectric dataset. Our results illustrate how new concepts can help articulate the difference between AL strategies, and how model accuracy does—and does not—relate to AL performance in discovering novel materials.

## 2 Active Learning for Single-objective Materials Discovery

AL is a specialized problem setting in machine learning related to optimal experimental design. [13, 23, 28] In the materials science context, consider a description  $\mathbf{x}$  of a material with corresponding observed property of interest  $y$ , thought to be linked by an unknown function  $f : \mathbf{x} \mapsto y$  which is expensive to evaluate, for example, synthesizing and characterizing a material. To systematically identify novel materials  $\mathbf{x}$  with desirable changes in  $y$ , a statistical (machine-learning) model  $\hat{f}$  is built that estimates (approximates, predicts) the unknown function  $f$ . Trained on an initial set of characterized materials  $\tilde{\mathcal{X}}_0 = \{\mathbf{x}_1, \dots, \mathbf{x}_{n_0}\}$  with measured properties  $\tilde{\mathcal{Y}}_0 = \{y_1, \dots, y_{n_0}\}$ , the initial model  $\hat{f}_0$  is used to select new candidate materials  $\mathbf{x}_{n_0+1}, \dots, \mathbf{x}_{n_0+n_1}$ . These are characterized and added to the dataset,  $\tilde{\mathcal{X}}_1 = \{\mathbf{x}_1, \dots, \mathbf{x}_{n_0+n_1}\}$ , which is then used to train a new improved model  $\hat{f}_1$ . This results in a sequence of datasets  $\tilde{\mathcal{X}}_k, \tilde{\mathcal{Y}}_k$  for  $k = 0, \dots, K$ . While this cycle can in principle be fully automated, new candidates are usually selected by domain experts based on AL suggestions (“human-in-the-loop”).

Various objectives can drive the design of AL strategies; for instance, a common objective in general machine learning is to improve the model  $\hat{f}$ . In materials informatics, the objective is often to identify an improved material  $\mathbf{x}$  using as few physical experiments as possible. [12] We call the design space of experimentally accessible, that is, synthesizable and measurable materials the *global scope*.

For a *single objective*, measuring the relative performance of candidates is straightforward (Fig. 2), as they can be ranked unambiguously based on their scalar performance, for example, strength-to-weight ratio for structural alloys. One way to measure the performance of AL is to retrospectively simulate AL on a known dataset and count the number of AL iterations necessary to reach a known top candidate. [12] A key decision in designing an AL method is the choice of *acquisition function*. We will discuss these in greater detail in Section 3; briefly, an acquisition function is a decision rule used to rank potential candidates in an AL context. Such criteria navigate the “exploration-exploitation” trade-off: [8] The algorithm should seek improved candidates, but should also try “risky” candidates to improve its model and enable later

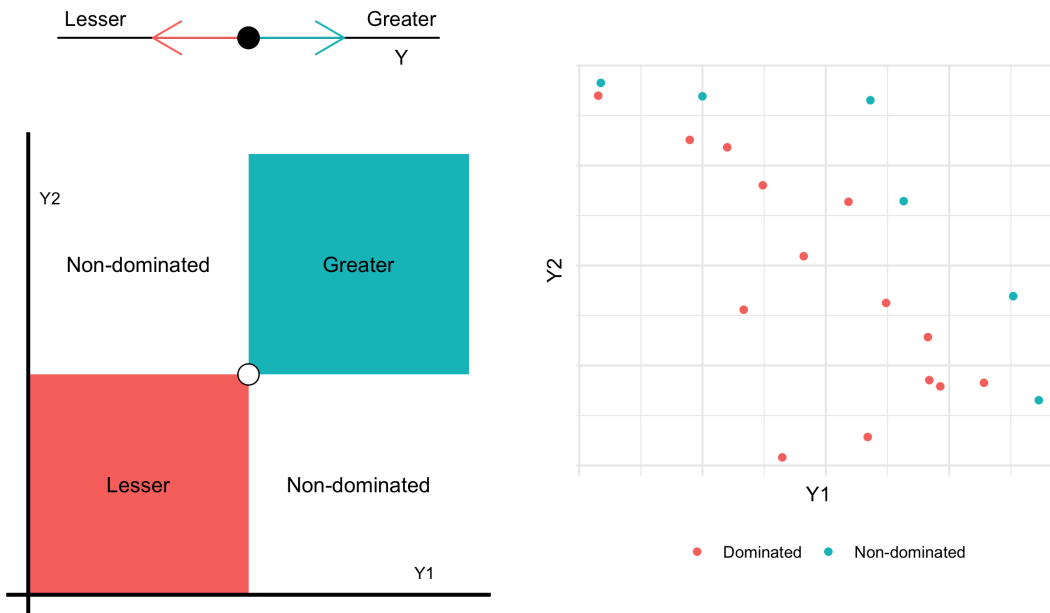


Figure 2: *Multi-objective optimization requires ranking concepts beyond “greater” and “lesser.”* Illustration of candidate ranking settings (Left) and an example multi-objective frontier (Right). In the single-objective setting, a relative ranking between candidates is always possible via the total ordering induced by the single objective. However, in the multi-objective setting, two candidates can be neither greater nor lesser than the other if they are alternately dominant along different objectives – two distinct candidates can be *non-dominated*. Recognizing this issue leads naturally to the notion of a *non-dominated set* of mutually incomparable candidates – the Pareto frontier. Here we consider maximization along both  $Y_1, Y_2$ ; the notion of Pareto dominance trivially generalizes to cases where minimization is desired along one or more axes (e.g. Fig. 3). (Figure inspired by Ref. [11, Fig. 12.1].)

discoveries. [22] Many improvement criteria for the single-objective case have been proposed and tested in the literature [1, 12, 20, 31, 33, 37]. The multi-objective setting, however, requires a more nuanced understanding of candidate ranking.

### 3 Multi-objective Methods

In multi-objective optimization, the categories of “greater” and “lesser” are insufficient (Fig. 2). Since two candidates compete along multiple axes, it is possible for two candidates to be mutually *non-dominated*. Multiple objectives occur naturally in materials science problems and are often unavoidable, e.g. the strength-toughness trade-off which arises from fundamental, competing effects [18]. In lieu of more preference information, one must navigate the resulting multi-objective trade space. Having access to more candidates in this trade space enables a more complete scientific understanding and more informed engineering decision making. In this section we review concepts from multi-objective optimization and introduce acquisition functions for the multi-objective setting.

#### 3.1 Dominance and strata

In the single-objective case, it is simple to objectively rank candidates  $y, y' \in \mathbb{R}$ . A candidate  $y$  is either lesser  $y < y'$ , greater  $y > y'$ , or equal  $y = y'$  to another candidate  $y'$ . However, the introduction of multiple objectives  $\mathbf{y}, \mathbf{y}' \in \mathbb{R}^D$  introduces new complexities. Figure 2 illustrates the universe of possible comparisons; in addition to lesser, greater, and equal, the multi-objective setting introduces the notion of *non-dominated*

points [11, Chapter 12]. *Dominance* (in the Pareto sense) is a pairwise relationship; the candidate  $\mathbf{y}$  is said to *dominate*  $\mathbf{y}'$  if

$$\begin{aligned} y_d &\geq y'_d \text{ for all } d \in \{1, \dots, D\}, \\ \text{and } y_d &> y'_d \text{ for some } d. \end{aligned} \tag{1}$$

We use the notation  $\mathbf{y}' \prec \mathbf{y}$  to denote that  $\mathbf{y}$  dominates  $\mathbf{y}'$ . Note that the definitions above pre-suppose that optimization is posed in terms of maximization of all objectives. This is not a limitation – if minimization is desired for a given axis  $y_d$ , then one must simply reverse the relevant inequalities in definition 1. Furthermore, proximity to a desired value can be encoded as minimization of absolute distance from the target value, e.g. bandgap as close as possible to 1.2eV.

In the multi-objective setting, the possibility of non-dominance implies that a single “best” multi-objective output value  $\mathbf{y}$  may not exist. Instead, there may be a set of “best values”. Given a set of candidates  $\mathcal{A} \subseteq \mathbb{R}^D$ , the set of non-dominated points is called the *Pareto frontier*, defined by

$$\mathcal{P}(\mathcal{A}) = \{\mathbf{y} \in \mathcal{A} \mid \forall \mathbf{y}' \in \mathcal{A}, \mathbf{y} \not\prec \mathbf{y}'\}. \tag{2}$$

The Pareto frontier  $\mathcal{P}(\mathcal{A})$  represents the set of tradeoffs one must navigate in choosing an optimization candidate. Further selection must be made through external considerations: possibly a prioritization of the objectives, or through less-quantifiable concerns such as the corrosion resistance of a material.

While the Pareto frontier is an important set of candidates, points outside the frontier are not without utility, particularly if aforementioned external concerns exist. Candidates near the frontier can be useful as training data for a machine learning model, while measurement or model uncertainties may lead to the false classification of a point as dominated. To describe points near the Pareto frontier, we use the notion of *strata*.

The *strata* are defined via a recursive relationship [19]. Let  $\mathcal{A}$  be a set of candidates as above, and define the  $s$ -th stratum  $\mathcal{S}_s$  via

$$\begin{aligned} \mathcal{S}_1 &= \mathcal{P}(\mathcal{A}), \\ \mathcal{S}_s &= \mathcal{P}(\mathcal{A} - \mathcal{S}_{s-1}) \text{ for } s = 2, \dots \end{aligned} \tag{3}$$

Figure 3 illustrates a few strata on the thermoelectrics dataset. Note that by definition, we have  $\mathcal{S}_i \cap \mathcal{S}_j = \emptyset$  if  $i \neq j$ . This allows us to define a *stratum number* for each point  $\mathbf{y} \in \mathcal{A}$  via

$$s(\mathbf{y}) = s \mid \mathbf{y} \in \mathcal{S}_s. \tag{4}$$

The candidates along the pareto frontier then have  $s(\mathbf{y}) = 1$ , while points with larger stratum number lie increasingly far from the Pareto frontier. We will use the stratum number to rank the performance of AL with greater resolution than counting frontier points alone.

We also define the *Pareto shell* via

$$\mathcal{P}_s = \bigcup_{j=1}^s \mathcal{S}_j. \tag{5}$$

This definition allows one to select a “band” of points along and near the Pareto frontier. Below, we will use the Pareto shell  $\mathcal{P}_s$  as a targeted scope for computing model accuracy. We use the nomenclature *s-Shell* to denote  $\mathcal{P}_s$ : Figure 3 illustrates a Pareto 4-Shell for the thermoelectric dataset.

### 3.2 Measuring performance

Prior work assessing AL in materials informatics has focused primarily on the number of Pareto frontier points acquired during AL [12, 24]. While certainly a relevant objective to pursue, this “all or nothing” measurement of success provides no accounting for candidates near the Pareto frontier, which may still be of scientific interest. This is particularly troublesome when studying datasets that have very few Pareto frontier points, such as the “sparse” frontier we will consider below. To provide a measure with more granularity, we consider the *mean stratum number* at each iteration of AL  $\mathcal{J}_k$ , using the ground truth strata from the full dataset.

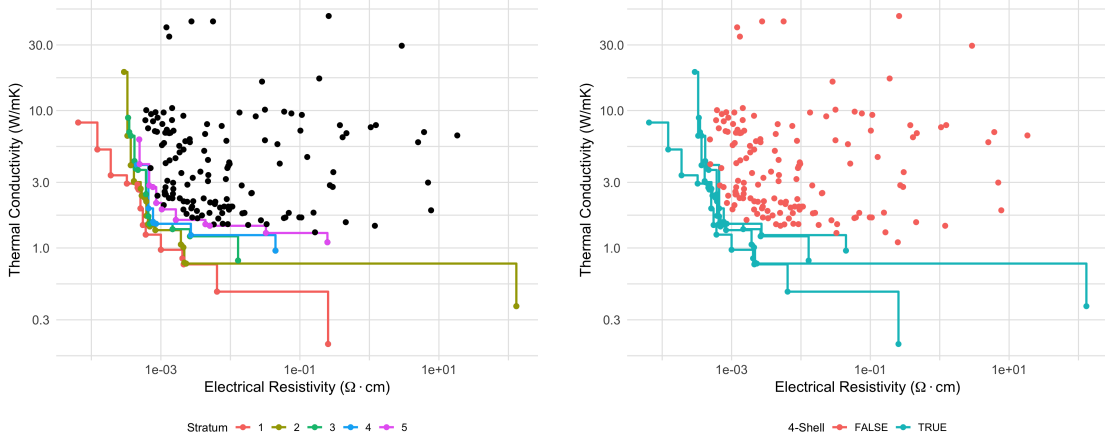


Figure 3: A recursive generalization of non-dominance (strata) enables a definition of scope tailored for optimal material candidates. Example of strata (left) and a Pareto shell (right) for the thermoelectric dataset, considering only  $\rho, \kappa$  for preference ranking (both minimized). The 1-st stratum corresponds to the Pareto frontier, while higher strata are the Pareto frontier of the recursive difference. Considering all strata up to a user-selected number  $N$  yields the Pareto  $N$ -shell. On the Right, we visualize an example 4-Shell, which consists of all the points in the first four strata. Below we will use the concept of Pareto shells to define an error scope relevant to AL for materials discovery.

In addition to the candidate improvement performance of AL, we also consider trajectories of model performance. We use the notion of *non-dimensional error* (NDE) across each of the output quantities; given a set of true  $\{\mathbf{y}_i\}_{i=1}^n = \mathcal{Y}$  and estimated  $\{\hat{\mathbf{y}}_i\}_{i=1}^n = \hat{\mathcal{Y}}$  response values, we compute the NDE for output  $d$  via

$$\bar{y}_d = \frac{1}{n} \sum_{i=1}^n y_{i,d},$$

$$NDE_d = \sqrt{\frac{\sum_{i=1}^n (y_{i,d} - \hat{y}_{i,d})^2}{\sum_{i=1}^n (y_{i,d} - \bar{y}_d)^2}}. \quad (6)$$

If we have  $D$  output quantities, then there are  $D$  NDE values to compute. Note that the NDE is closely related to the *coefficient of determination*  $R^2$  via the expression  $NDE = \sqrt{1 - R^2}$  [36]. Since the NDE is dimensionless, we may safely average NDE values across the  $D$  outputs to compute a *mean non-dimensional error* (MNDE), given by

$$MNDE = \frac{1}{D} \sum_{d=1}^D NDE_d. \quad (7)$$

Given the simulation nature of our test cases, the Global-scope error is naturally evaluated by expression (6) across the entire dataset. However, this *Global-scope* includes regions of output space that are not emphasized in our frontier-seeking context. To compute error metrics with *targeted scope*, we use the notion of a Pareto shell to compute error on the relevant portions of the output domain (e.g. Fig. 3). This notion of scope is closely related to the concept of a *domain of applicability*, with the contrast that the scope is defined by the analyst, whereas the aforementioned domain is identified from a trained machine learning model [26]. We will denote the scope of an error calculation via subscript, such as  $MNDE_{\text{Global}}$  and  $MNDE_{2\text{-Shell}}$ .

$[\rho] = \text{Ohm} \cdot \text{cm}$	$[\rho] = \text{Ohm} \cdot \text{m}$
1	185
2	1
3	2
4	3

Table 1: A lack of dimensional homogeneity in acquisition function logic can lead to non-robust decisions. Example ranks computed via Euclidean distances under different choices of unit systems, using the thermoelectric dataset. Note that the rank distance from a reference point (the origin) is different, depending on the choice of units used to express the thermal resistivity  $\rho$ . This demonstrates that using distance to rank candidates in a multi-objective space with physical quantities leads to decisions that vary with the user-selected unit system.

### 3.3 Acquisition functions

Given the multivariate nature of the output space  $\mathbf{y} \in \mathbb{R}^D$ , we must introduce some form of decision criteria that summarizes available information about material candidates, and returns a ranking for selecting promising new selections. To that end, we define an *acquisition function*  $f_a(\mathbf{x}; \mathcal{M})$  as any function which is used to select an optimal candidate via

$$\mathbf{x}^* = \arg \max_{\mathbf{x} \in \tilde{\mathcal{X}}^C} f_a(\mathbf{x}; \mathcal{M}) \quad (8)$$

where  $\mathcal{M}$  is a trained machine learning model which returns both a prediction  $\hat{\mathbf{y}}$  and a predictive distribution  $\mathbf{Y} \sim \mathcal{D}$ , both of which are available to the acquisition function  $f_a$ .

Many generalizations of single-objective acquisition functions are available from the literature, including the probability of improvement and expected improvement criteria [10], the maxmin criterion [27], and the expected hyper-volume improvement (EHVI) criterion [24]. Our aim in this work is not to compare these and other criteria; instead, we are focused on 1. How the fidelity with which the Pareto frontier is represented relates to AL performance, and 2. how optimal candidate selection is (or is not) related to model accuracy. Below, we introduce the acquisition functions to be studied in this work, but first provide a remark on dimensional homogeneity.

**Importance of dimensional homogeneity** Before introducing specific acquisition functions, we first make a remark on the importance of *dimensional homogeneity*. In order to measure the performance of multiobjective AL, we may wish to measure the “distance” of candidates to the Pareto frontier. However, we will see here that a naive notion of distance is problematic, as it does not respect dimensional homogeneity – the ranking results are not independent of the analyst’s choice of unit system.

To illustrate, let  $\mathbf{y}, \mathbf{y}' \in \mathbb{R}^D$ , where the  $y_d$  potentially have different physical units. The ordinary notion of distance is given by

$$\|\mathbf{y} - \mathbf{y}'\|_p = \left( \sum_{d=1}^D |y_d - y'_d|^p \right)^{1/p}. \quad (9)$$

Note that for all  $p \in (0, +\infty)$ , the expression  $\|\mathbf{y} - \mathbf{y}'\|_p$  involves the addition of terms of potentially dissimilar physical units. This expression violates dimensional homogeneity, which introduces an artificial dependence on the chosen unit system. Table 1 demonstrates a consequence of this lack of homogeneity – the ranks computed by Euclidean distances are not stable to a change of unit system. This illustrates that arbitrary choices can drastically affect decisions based on this sort of distance computation. To overcome this issue, we only consider acquisition functions that respect dimensional homogeneity.

**Uncertainty sampling** *Uncertainty sampling* leans towards the exploration side of AL, and chooses candidates based on where the model is most uncertain. In the scalar case, this is easily accomplished by choosing the candidate with the greatest predictive variance  $\hat{\sigma}_i^2$  [22]. This approach does not immediately

generalize to the multi-objective case, as the component variances  $\hat{\sigma}_{i,d}^2 = \hat{\Sigma}_{i,dd}$  do not necessarily have the same units. To respect dimensional homogeneity, we generalize uncertainty sampling by considering a sum of dimensionless quantities.

**Sum of Coefficients of Variation (SCV):** The SCV is defined via

$$f_{SCV}(\mathbf{x}_i) = \sum_{d=1}^D \text{COV}_{i,d}, \quad (10)$$

$$\text{COV}_{i,d} = \hat{\sigma}_{i,d} / \hat{\mu}_{i,d},$$

where  $\hat{\mu}_{i,d}, \hat{\sigma}_{i,d}$  are the  $d = 1, \dots, D$  components of the mean and standard deviation of the predictive distribution  $\hat{\mathcal{D}}_i$ . The coefficients of variation  $\text{COV}_{i,d}$  are dimensionless quantities, with a normalizing scale  $\hat{\mu}_{i,d}$  set not by the user, but rather by the available data.

**Frontier modeling strategies** Here we introduce a family of acquisition functions that seek improvement over an existing Pareto frontier, in order of increasing fidelity with which they model the Pareto frontier. Each of these strategies is a form of probability statement; by construction, these quantities respect dimensional homogeneity.

**Probability of Joint Exceedance (PJE):** The PJE is defined via

$$f_{PJE}(\mathbf{x}_i) = \mathbb{P}_{\mathcal{D}_i}[Y_{i,d} > \max_{\mathbf{y} \in \mathcal{Y}} y_d], \quad (11)$$

where  $\mathbf{Y}_i \sim \hat{\mathcal{D}}_i$  is the random variable which follows the predictive distribution  $\hat{\mathcal{D}}_i$  for candidate  $i$ . In words, definition (11) is the probability that candidate  $\mathbf{Y}_i$  will exceed the performance observed in our existing training data  $\mathcal{Y}$  along every axis of comparison. This is a very “aggressive” acquisition function that ignores much of the structure of the Pareto frontier. Figure 4 illustrates the PJE, alongside the other frontier modeling criteria.

**Hyperplane Probability of Improvement (HPI):** The HPI is defined in terms of a hyperplane fit of the Pareto frontier in the available training data. Modeling the Pareto frontier as a hyperplane requires fitting a normal direction  $\hat{\mathbf{w}} \in \mathbb{R}^D$  and an offset  $\hat{b}$ . Once these are fit, the HPI is defined in terms of the appropriate Z-score via

$$f_{HPI}(\mathbf{x}_i) = \frac{\hat{\mathbf{w}}^\top \hat{\boldsymbol{\mu}}_i - \hat{b}}{\sqrt{\hat{\mathbf{w}}^\top \hat{\Sigma}_i \hat{\mathbf{w}}}}. \quad (12)$$

In words, the HPI is the probability that a candidate  $\mathbf{Y}_i$  will present improvement over the hyperplane fit of the existing Pareto frontier.

There are many ways to fit a hyperplane to a set of data. One option is to arbitrarily select one output  $Y_i$  and perform linear regression using the remaining outputs as regression variables. We recommend against this approach, as it suffers from the *regression fallacy* [15, Ch. 9.1]. In practice, we perform a principal component analysis of the available Pareto frontier data, and use the least-variance direction to define the hyperplane direction  $\hat{\mathbf{w}}$ . Together with the mean of the Pareto frontier data  $\bar{\mathbf{Y}}$ , we then define the offset via  $\hat{b} = \hat{\mathbf{w}}^\top \bar{\mathbf{Y}}$ .

Figure 4 illustrates the HPI: Note that this definition assumes a hyperplane structure, which will not be appropriate for all Pareto frontiers. Further, the HPI “fills in” the staircase structure posed by the true Pareto frontier – our final frontier modeling acquisition function captures this structure.

**Probability Non-Dominated (PND):** The PND is defined via

$$f_{PND}(\mathbf{x}_i) = \mathbb{P}_{\mathcal{D}_i}[Y_i \not\prec \mathbf{y}, \forall \mathbf{y} \in \mathcal{Y}], \quad (13)$$

with dominance  $\prec$  defined in (1). In words, the PND computes the probability that a given candidate  $\mathbf{Y}_i$  will be non-dominated with respect to the available data. This criterion is studied in approximate form in reference [10]. The PND considers the available Pareto frontier in full-fidelity, introducing no modeling assumptions. Figure 4 illustrates this acquisition function against the aforementioned definitions.

Note that while PND captures the true geometry of the Pareto frontier, since the frontier is allowed to have quite general structure, no simple analytic expression like PJE or HPI exists. Instead, one may

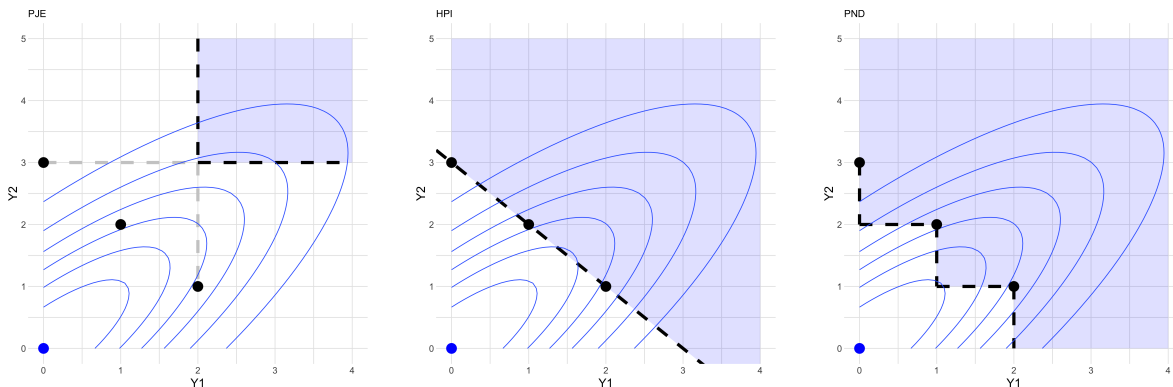


Figure 4: Schematics illustrating the acquisition functions probability of joint exceedance (PJE, Left), hyper-plane probability of improvement (HPI, Center), and probability non-dominated (PND, Right) for the same candidate (blue) and frontier points (black). Both outputs  $Y1, Y2$  are to be maximized. The blue curves depict equi-likelihood contours for a single candidate’s predictive density  $\hat{\mathcal{D}}$ . The shaded region depicts the region that is integrated for the respective acquisition function. Note that PJE largely ignores the frontier geometry, HPI crudely models the Pareto frontier, and PND accurately considers the Pareto frontier.

approximate the PND via simple Monte Carlo, drawing samples from the predictive distribution  $\mathcal{D}_i$  and counting the proportion that are non-dominated. This leads to a greater computational expense to evaluate the PND, as compared with PJE or HPI. The experiments below will demonstrate that this added expense is valuable if higher AL performance is desired.

## 4 Results

### 4.1 Test cases

To compare the acquisition functions introduced above, we simulate AL on a collection of synthetic and real test cases. The synthetic cases are constructed to present different Pareto frontier geometries, including a simple linear frontier, and examples of convex and concave frontiers. We also construct a “sparse” frontier containing relatively few low-stratum points; there are just five Pareto frontier points in the “Hyperbolic” dataset. Figure 5 depicts these test-cases’ two-dimensional output space. The functional forms for these models are given in Appendix 6.1.

We also consider a real dataset of thermoelectric materials, depicted in Figure 6 [5]. The performance (property) space consists of thermal conductivity  $\kappa$ , electrical resistivity  $\rho$ , and the Seebeck coefficient  $S$ . The inputs are computed using the Magpie featurization library [34, 35].

### 4.2 Simulated active learning

The primary evidence of this work is based on a battery of AL simulations, which support the comparison of different acquisition functions against a common setup. For all experiments, we use the random forest model implemented in *lolo* [7].

In practice, performing AL for materials discovery is rife with uncertainties. Chance phenomena such as initial data selection can affect the results, implying that single runs of active learning are insufficient for measuring performance. We consider an ensemble of runs against a randomized selection of initial data, in order to provide a robust estimate of relative performance.

To perform a single run of AL, we carry out the following steps:

1. Choose an initial random subset  $\tilde{\mathcal{X}}_0 \subseteq \mathcal{X}$  of size  $|\tilde{\mathcal{X}}_0| = C$  for the training data, and reveal the paired labels  $\tilde{\mathcal{Y}}_0$  to the simulation. Set the iteration counter to  $k = 0$ .
2. Fit a machine learning model to the available paired data  $\tilde{\mathcal{X}}_k, \tilde{\mathcal{Y}}_k$ . This returns predictions  $\hat{\mathbf{y}}_i$  and predictive densities  $\hat{\mathcal{D}}_i$ .



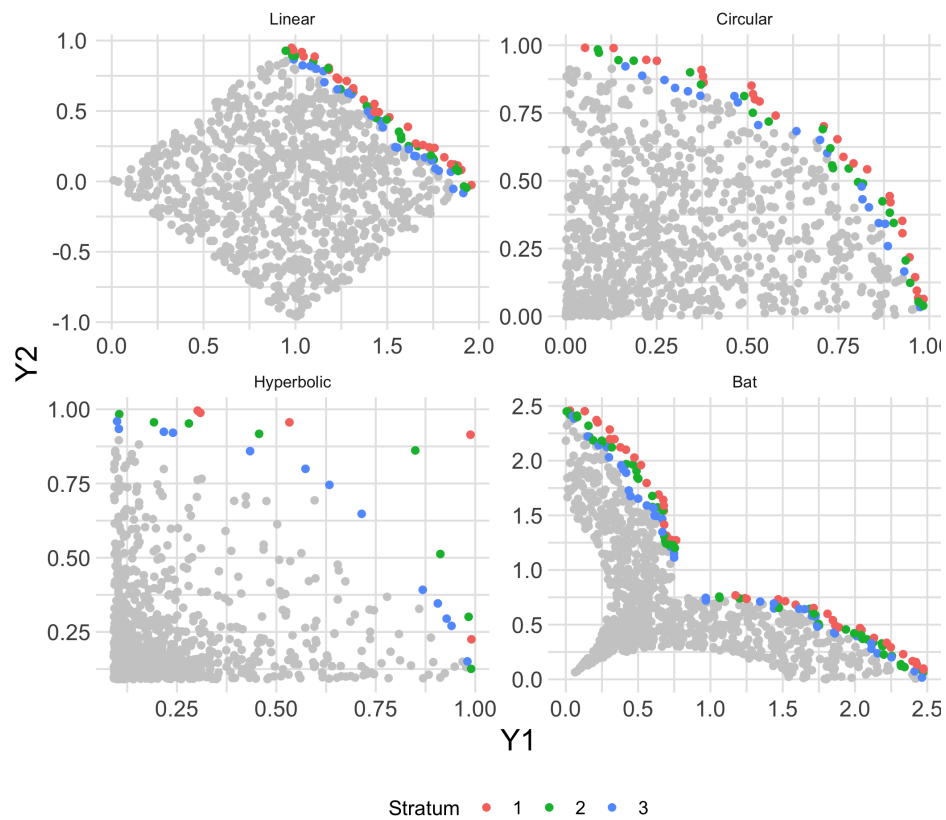


Figure 5: Lineup of synthetic test cases in terms of their output (property) spaces. Each output space is two-dimensional, with both outputs to be maximized. Note that each test case has a different Pareto frontier geometry, including convex (Circular), concave (Bat), and sparse (Hyperbolic) examples.

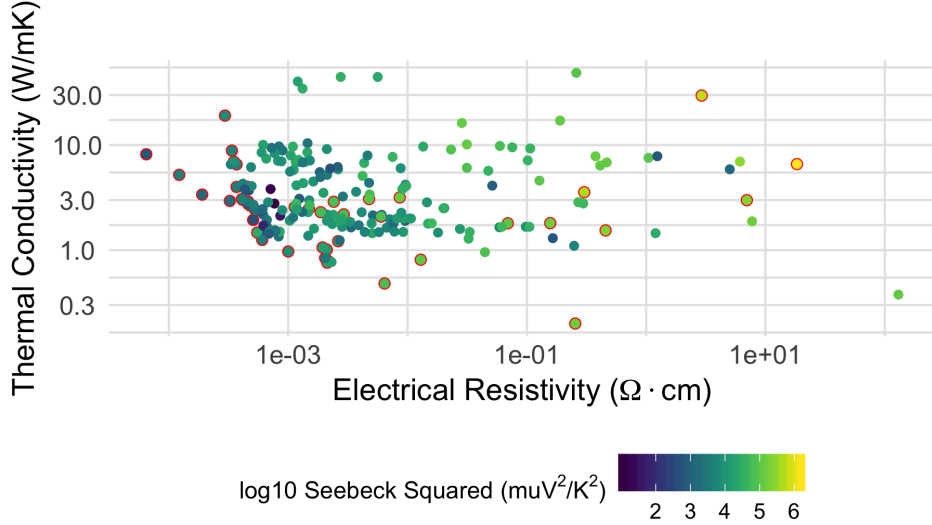


Figure 6: Output (property) space for the thermoelectric dataset. Outputs Thermal Resistivity and Electrical Conductivity are to be minimized, while the squared-Seebeck coefficient is to be maximized. Pareto frontier points are highlighted in red.

3. Rank the candidates remaining in the dataset  $\mathbf{x}_i \in (\mathcal{X} - \tilde{\mathcal{X}}_k)$  according to the chosen acquisition function  $f_a(\mathbf{x}_i)$ . Select the top-performing candidate  $\mathbf{x}^*$ , and add it to the database  $\tilde{\mathcal{X}}_{k+1} = \tilde{\mathcal{X}}_k + \{\mathbf{x}^*\}$ . Reveal the label for  $\mathbf{x}^*$  to the simulation.
4. Repeat from Step 2 for  $k = 1, \dots, K - 1$  iterations.

To perform an ensemble of AL runs, we select different random subsets  $\tilde{\mathcal{X}}_{0,1}, \dots, \tilde{\mathcal{X}}_{0,R}$  for  $R$  replications, and aggregate results across these runs. In practice, we vary the initial candidate pool size  $C$ , the total number of iterations  $K$ , the considered test case, and the chosen acquisition function. Results from this database of simulations are reported below.

### 4.3 Candidate improvement

Here we report results on candidate discovery performance. We consider both the usual metric of the number of non-dominated points (NNDP) acquired (Fig. 7) and the proposed measure of mean stratum (Fig. 8). Across all test-cases considered, we have found that MPND, MHPI, and MPJE are ranked in descending order with respect to NNDP performance—the same descending order of Pareto frontier modeling fidelity. Ranking results for the same criteria are mixed for shorter-term performance. These results suggest that capturing the true geometry of the Pareto frontier is most important in “later stage” AL, where the space of candidates is limited.

The difference in “early stage” performance is better revealed by the mean stratum results (Fig. 8). In the early stages of AL MHPI tends to give the best performance, delivering more candidates at-or-near the Pareto frontier. The reason for this difference is explained in Subsection 4.5 below, which analyzes qualitative performance.

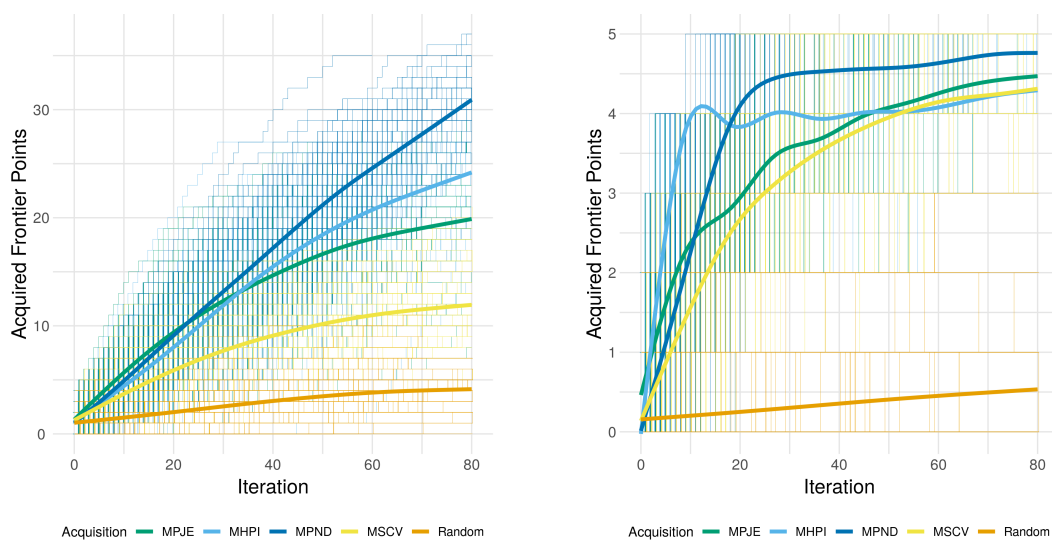


Figure 7: *Greater acquisition function fidelity leads to more non-dominated candidates.* Total frontier points acquired for the Bat (Left) and Hyperbolic (Right) synthetic frontiers. Uncertainty sampling (MSCV) has unreliable performance, performing marginally better than Random search on the Bat frontier, but performing well on the Hyperbolic test case. In terms of long-run performance, the criteria MPJE, MHPI, and MPND tend to rank in the same order as the fidelity with which they represent the Pareto frontier. As seen in Figure 1, MPND also out-performs other criteria on the thermoelectric dataset in terms of long-run performance. These results suggest that incorporating high-fidelity modeling of the Pareto frontier to acquisition function is particularly important in well-studied problems with few possible candidates. Finally, note that the Hyperbolic test-case has only 5 non-dominated candidates total—this fundamentally limits the resolution of AL results for this case. Figure 8 analyzes the same AL results in terms of mean stratum number, which reveals other trends in the same data.

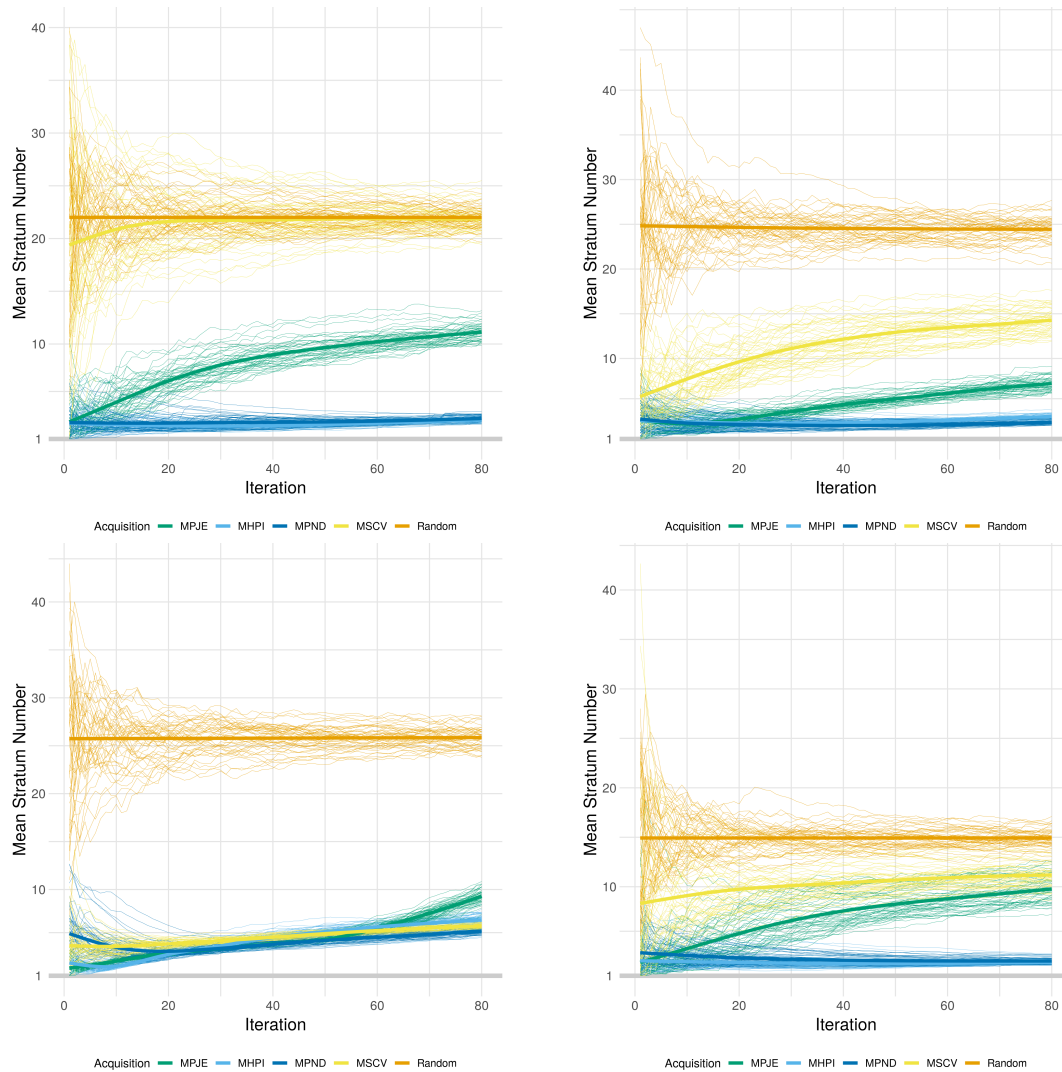


Figure 8: *Mean stratum number highlights trends not captured by the number of non-dominated points (NNDP)*. Results shown for the Linear (Top-Left), Circular (Top-Right), Hyperbolic (Bottom-Left) and Bat (Bottom-Right) synthetic frontiers. Computing the mean stratum number reveals that the MHPI criterion acquires more near-frontier points than MPND in the early stages of AL, with a slight edge in the Bat case, and a decisive advantage in the Hyperbolic case. In the later stages of AL, MPND tends to dominate. Compared to NNDP results (Fig. 7), these mean stratum results highlight that the non-random criteria have similar performance on the Hyperbolic case for the middle of AL runs. Note that MPJE performance tends to saturate earlier than other criteria, rather than ranking second when performance is measured with the NNDP metric—this suggests MPJE begins selecting candidates far from the Pareto frontier in later-stage AL, a hypothesis confirmed in Figures 11 and 12.

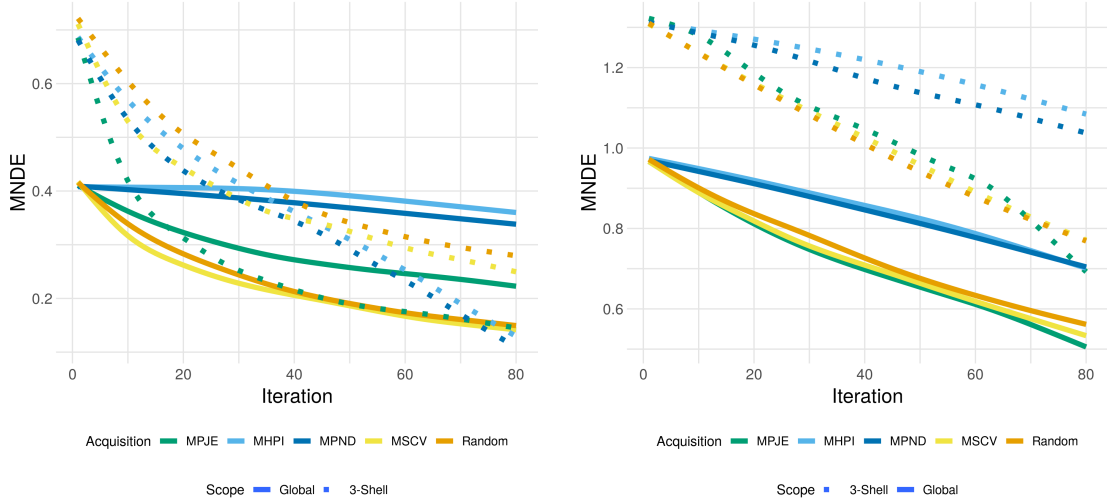


Figure 9: *Best model accuracy improvement through active learning depends on error scope as well as acquisition function.* Mean non-dimensional error (MNDE) at different scopes (solid for Global, dots for Shell) for the Linear (Left) and thermoelectric (Right) cases. The MSCV and Random selection criteria tend to result in strong error reduction in terms of Global-scope across most test-cases. However, MPND tends to give the most consistent long-run performance in shell scope for the synthetic cases. Note that in the Linear test-case, MPJE tends to achieve early gains for shell error, but saturates in performance as the criteria fails to spread across the Pareto frontier (Figs. 11 and 12). The thermoelectric dataset bucks these trends, showing similar error behavior in both scopes.

#### 4.4 Model improvement

Here we report results on how model accuracy evolves during AL. Figure 9 summarizes consistent trends across all synthetic cases considered: The Random and MSCV (uncertainty sampling) criteria tend to best improve model error in a Global-scope, while MPND, MHPI, and MPJE tend to best improve error in the Shell-scope. Generally MPJE gives a short-term reduction in Shell-scope error but reaches a plateau. The MPND and MHPI criteria give better long-term Shell-scope error reduction. Note that these trends do not persist for the thermoelectric dataset; based on the absolute magnitude of MNDE values for this case, we can tell that the model generally represents the data crudely. In this real-data case, the error reduction trends are similar across Global- and Shell-scopes.

We also directly connect model error with candidate improvement in Figure 10: We consider the Spearman (rank) correlation between MNDE values and the next-step acquisition stratum number, in order to probe for monotonic relations between the quantities [25]. A positive rank correlation indicates that decreasing error is associated with decreasing stratum—model improvement is then associated with candidate improvement. We employ the Fisher transform to approximate 99% confidence intervals for these correlations [2]. These results suggest that model error provides positive signal of AL performance only under narrow conditions: We find a significantly positive rank correlation with the Shell-scope error only when sufficiently many candidates are available for the algorithm to discover, the acquisition function is either MPND or MHPI, and the machine learning model is sufficiently informative (has reasonably low Shell-scope error).

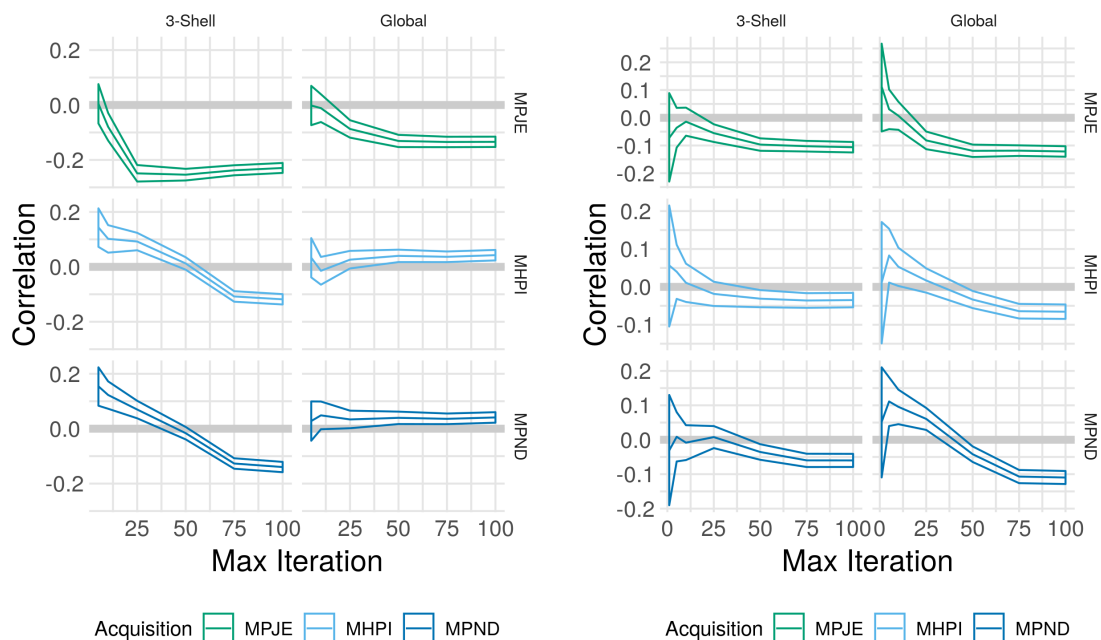


Figure 10: *Global-scope error is generally a poor indicator for active learning performance; Shell-scope error is conditionally predictive.* Spearman (rank) correlation between iteration-wise mean non-dimensional error  $MNDE_i$  and next-acquisition stratum number  $s(\mathbf{y}_{i+1})$  for Linear (Left) and thermoelectric (Right) data. A positive correlation indicates that lower error at step  $i$  is associated with acquiring lower-stratum materials candidates in step  $i + 1$ —positive signal that active learning for materials discovery will be successful. Mean estimates and 99% confidence intervals are reported at different cumulative fractions of the available data—correlation estimates with bounds overlapping zero do not confidently provide signal for AL performance. For the Linear test case, low shell error provides positive signal for the MHPI and MPND criteria, but only at low Max Iterations. Once all Pareto points have been acquired, the algorithm has exhausted all possibilities for improvement and resorts to acquiring lesser candidates, as signaled by negative correlation. However, model error does not always provide usable (positive) signal, as is the case in the real-data thermoelectric case where the correlation is not reliably greater than zero.

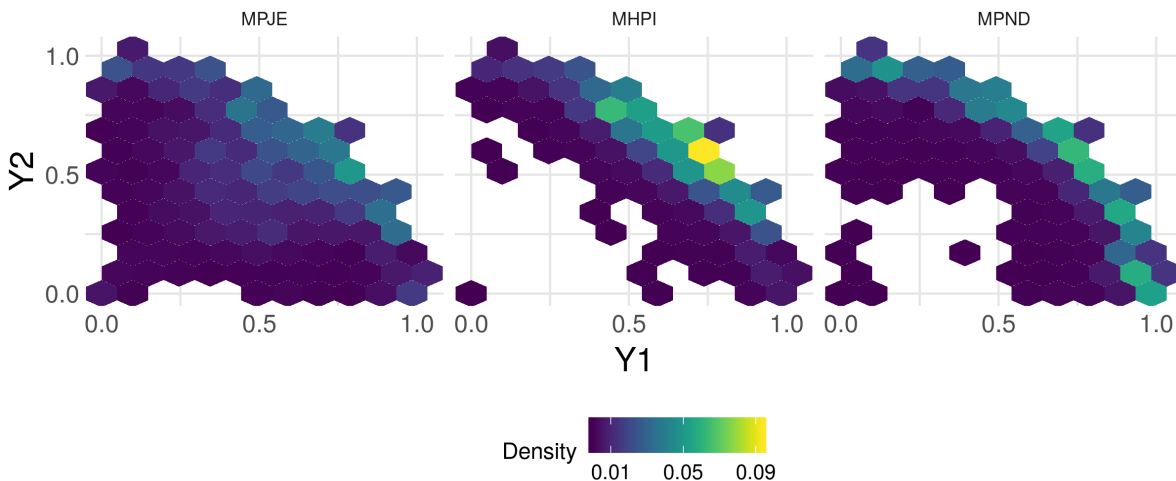


Figure 11: *Higher-fidelity acquisition functions explore the output space more thoroughly.* Density of selected points across all AL runs on the Circular case, faceted by acquisition functions. Note that the selections made according to MPJE are scattered among the entire domain, as compared with MHPI and MPND. MPND tends to distribute its selections along the entire Pareto frontier, as opposed to MHPI, which concentrates on the center of the frontier. Note also that MPND has wider support than MHPI, indicating that the former criteria tends to (infrequently) select more strongly dominated candidates than the later.

## 4.5 Qualitative performance

Here we report how the acquisition functions of Subsection 3.3 behave in terms of qualitative performance: where their selections tend to lie in output space. Figures 11 and 12 report empirical densities for selected candidates in output space. Broadly, MPJE tends to select candidates throughout the output space, MHPI focuses on “hotspots” along the frontier, and MPND thoroughly explores the frontier but infrequently selects strongly-dominated candidates. This qualitative analysis helps to explain the discrepancy in NNDP (Fig. 7) and mean stratum (Fig. 8) performance: MPND is able to explore the frontier thoroughly, selecting many non-dominated points. However, MPND is also more liable than MHPI to select strongly non-dominated candidates, leading to a higher mean shell number. Conversely, MHPI tends to concentrate its selections closer to a limited region of the Pareto frontier, leading to fewer possible non-dominated selections but a lower mean stratum.

## 5 Conclusions

In this work, we explored the relationship between different aspects of machine learning accuracy and candidate acquisition in multi-objective materials discovery. We showed that AL schemes which optimize for the usual notion of model accuracy – Global-scope error – do not guarantee optimal candidate discovery. To ameliorate the situation we introduced Pareto Shell-scope error, which we found to be more closely associated with discovering improved candidates.

We also studied the relationship between the accuracy with which acquisition functions represent the Pareto frontier and AL performance. We demonstrated that dimensionally-inhomogeneous acquisitions functions can lead to non-robust decision making, and so limited our attention to dimensionally-homogeneous acquisition functions. We found that the long-run discovery of non-dominated candidates was improved by modeling the Pareto frontier with greater fidelity. However, an acquisition function which rendered the Pareto frontier with lesser fidelity (MHPI) uncovered more candidates at-or-near the Pareto frontier in the early stages of AL, leading to a lower mean stratum number than the highest fidelity acquisition function

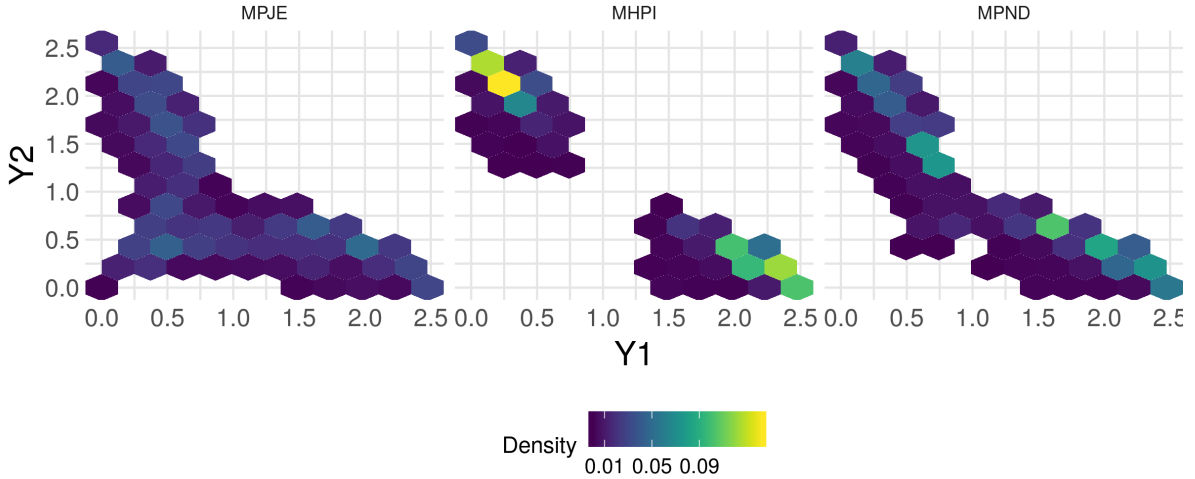


Figure 12: *Higher-fidelity acquisition functions explore the output space more thoroughly.* Density of selected points across all AL runs on the Bat case, faceted by acquisition functions. As with the Circular test case (Fig. 11), MPJE selects strongly-dominated candidates. MHPI focuses on the edges of the Pareto frontier, while MPND selects more evenly across the frontier. In contrast with the Circular case, the MHPI “hot-spots” are now at the edges of the Pareto frontier, rather than the center. MPND has non-zero support in the center of available candidates, another region of well-dominated points that contribute to a lower mean stratum number.

(MPND). We found that these acquisition functions tended to select material candidates at varying locations along the Pareto frontier with different frequency, leading to preferred “hot-spots” in material property space.

These results have ramifications for materials scientists seeking to use AL for materials discovery. Since Global-scope error is not always predictive of optimal candidate discovery, an analyst should check both Global- and Shell-scope error when deciding whether a model is sufficiently accurate to be used to rank materials candidates.

The selection of an appropriate acquisition function is highly dependent on the analyst’s goals. Based on our results, accurately modeling the Pareto frontier in an acquisition function is not critical for early-stage AL; that is, if the problem has a very large set of uncharacterized material candidates. Accurately capturing the Pareto frontier in the acquisition function logic becomes important when the design space is more thoroughly explored. In the absence of more specific preference criteria than non-dominated, the maximum probability non-dominated (MPND) strategy is the most performant among the acquisition functions tested here.

There are a number of remaining questions related to the present topic. In this work we fit independent models to all output quantities: Prior work suggests that modeling improvements can be made by accurately capturing output dependence structure among output quantities [3]. It would be interesting to study whether similar improvements can be found in AL performance. A conceptually different way to treat the multi-objective setting is to turn some objectives into constraints; it would be very interesting to compare the constrained approach against a multi-objective acquisition function in terms of mean stratum (c.f. Fig. 8) and acquisition densities (c.f. Fig. 11 and 12). Similarly, it would be interesting to compare performance across AL strategies using different scalarizations of the multi-objective space; e.g. the thermoelectric figure of merit  $zT$ .



## References

- [1] R Aggarwal, MJ Demkowicz, and YM Marzouk. Information-driven experimental design in materials science. In *Information Science for Materials Discovery and Design*, pages 13–44. Springer, 2016.
- [2] Ronald A Fisher. Frequency distribution of the values of the correlation coefficient in samples from an indefinitely large population. *Biometrika*, 10(4):507–521, 1915.
- [3] Thomas E Fricker, Jeremy E Oakley, and Nathan M Urban. Multivariate gaussian process emulators with nonseparable covariance structures. *Technometrics*, 55(1):47–56, 2013.
- [4] Estefanía Garijo del Río, Jens Jørgen Mortensen, and Karsten W. Jacobsen. Local Bayesian optimizer for atomic structures. *Physical Review B*, 100(10):104103, 2019.
- [5] Michael W Gaultois, Taylor D Sparks, Christopher KH Borg, Ram Seshadri, William D Bonificio, and David R Clarke. Data-driven review of thermoelectric materials: performance and resource considerations. *Chemistry of Materials*, 25(15):2911–2920, 2013.
- [6] Konstantin Gubaev, Evgeny V. Podryabinkin, Gus L. W. Hart, and Alexander V. Shapeev. Accelerating high-throughput searches for new alloys with active learning of interatomic potentials. *Computational Materials Science*, 156:148–156, 2019.
- [7] Maxwell Hutchinson. Lolo, 2016. accessed: 2019-07-01.
- [8] Mathias S. Jørgensen, Uffe Furlig Larsen, Karsten W. Jacobsen, and Bjørk Hammer. Exploration versus exploitation in global atomistic structure optimization. *Journal of Physical Chemistry A*, 122(5):1504–1509, 2018.
- [9] Shenghong Ju, Takuma Shiga, Lei Feng, Zhufeng Hou, Koji Tsuda, and Junichiro Shiomi. Designing nanostructures for phonon transport via Bayesian optimization. *Physical Review X*, 7(2):021024, 2017.
- [10] Andy J Keane. Statistical improvement criteria for use in multiobjective design optimization. *AIAA journal*, 44(4):879–891, 2006.
- [11] Mykel J Kochenderfer and Tim A Wheeler. *Algorithms for optimization*. MIT Press, 2019.
- [12] Julia Ling, Maxwell Hutchinson, Erin Antono, Sean Paradiso, and Bryce Meredig. High-dimensional materials and process optimization using data-driven experimental design with well-calibrated uncertainty estimates. *Integrating Materials and Manufacturing Innovation*, 6(3):207–217, 2017.
- [13] Douglas C. Montgomery. *Design and Analysis of Experiments*. Wiley, 9 edition, 2017.
- [14] Masanobu Nakayama, Kenta Kanamori, Koki Nakano, Randy Jalem, Ichiro Takeuchi, and Hisatsugu Yamasaki. Data-driven materials exploration for Li-ion conductive ceramics by exhaustive and informatics-aided computations. *The Chemical Record*, 19(4):771–778, 2019.
- [15] Art Owen. Stats 305 notes, 2013.
- [16] Daniel Packwood. *Bayesian Optimization for Materials Science*, volume 3 of *Springer Briefs in the Mathematics of Materials*. Springer Nature, Singapore, Singapore, 2017.
- [17] Daniel Packwood and Taro Hitosugi. Rapid prediction of molecule arrangements on metal surfaces via Bayesian optimization. *Applied Physics Express*, 10(6):065502, 2017.
- [18] Robert O Ritchie. The conflicts between strength and toughness. *Nature materials*, 10(11):817, 2011.
- [19] Patrick Roocks. Computing Pareto Frontiers and Database Preferences with the rPref Package. *The R Journal*, 8(2):393–404, 2016.
- [20] Atsuto Seko, Tomoya Maekawa, Koji Tsuda, and Isao Tanaka. Machine learning with systematic density-functional theory calculations: Application to melting temperatures of single-and binary-component solids. *Physical Review B*, 89(5):054303, 2014.

- [21] Atsuto Seko, Atsushi Togo, Hiroyuki Hayashi, Koji Tsuda, Laurent Chaput, and Isao Tanaka. Prediction of low-thermal-conductivity compounds with first-principles anharmonic lattice-dynamics calculations and Bayesian optimization. *Physical Review Letters*, 115(20):205901, 2015.
- [22] Burr Settles. Active learning literature survey. Technical report, University of Wisconsin-Madison Department of Computer Sciences, 2009.
- [23] Burr Settles. *Active Learning*, volume 18 of *Synthesis Lectures on Artificial Intelligence and Machine Learning*. Morgan & Claypool, 2012.
- [24] Alexandros Solomou, Guang Zhao, Shahin Boluki, Jobin K Joy, Xiaoning Qian, Ibrahim Karaman, Raymundo Arróyave, and Dimitris C Lagoudas. Multi-objective bayesian materials discovery: Application on the discovery of precipitation strengthened niti shape memory alloys through micromechanical modeling. *Materials & Design*, 160:810–827, 2018.
- [25] C. Spearman. The proof and measurement of association between two things. *The American Journal of Psychology*, 15(1):72–101, 1904.
- [26] Christopher A Sutton, Mario Boley, Luca M Ghiringhelli, Matthias Rupp, Jilles Vreeken, and Matthias Scheffler. Identifying domains of applicability of machine learning models for materials science. *ChemRxiv*, 2019.
- [27] Joshua Svenson and Thomas Santner. Multiobjective optimization of expensive-to-evaluate deterministic computer simulator models. *Computational Statistics & Data Analysis*, 94:250–264, 2016.
- [28] Anjana Talapatra, Shahin Boluki, Thien Duong, Xiaoning Qian, Edward Dougherty, and Raymundo Arróyave. Autonomous efficient experiment design for materials discovery with Bayesian model averaging. *Physical Review Materials*, 2(11):113803, 2018.
- [29] Milica Todorović, Michael U. Gutmann, Jukka Corander, and Patrick Rinke. Bayesian inference of atomistic structure in functional materials. *Nature Partner Journal Computational Materials*, 5:35, 2019.
- [30] Kevin Tran and Zachary W. Ulissi. Active learning across intermetallics to guide discovery of electrocatalysts for CO<sub>2</sub> reduction and H<sub>2</sub> evolution. *Nature Catalysis*, 1(9):696–703, 2018.
- [31] Tsuyoshi Ueno, Trevor David Rhone, Zhufeng Hou, Teruyasu Mizoguchi, and Koji Tsuda. Combo: an efficient bayesian optimization library for materials science. *Materials discovery*, 4:18–21, 2016.
- [32] Tsuyoshi Ueno, Trevor David Rhone, Zhufeng Hou, Teruyasu Mizoguchi, and Koji Tsuda. COMBO: An efficient Bayesian optimization library for materials science. *Materials Discovery*, 4:18–21, 2016.
- [33] Yingfei Wang, Kristofer G Reyes, Keith A Brown, Chad A Mirkin, and Warren B Powell. Nested-batch-mode learning and stochastic optimization with an application to sequential multistage testing in materials science. *SIAM Journal on Scientific Computing*, 37(3):B361–B381, 2015.
- [34] Logan Ward, Ankit Agrawal, Alok Choudhary, and Christopher Wolverton. A general-purpose machine learning framework for predicting properties of inorganic materials. *npj Computational Materials*, 2:16028, 2016.
- [35] Logan T. Ward, Alex Dunn, Alireza Faghaninia, Nils E. R. Zimmermann, Saurabh Bajaj, Qi Wang, J. E Paredes Montoya, Jiming Chen, Kyle Bystrom, Maxwell T. Dylla, Kyle Chard, Mark Asta, Kristin A. Persson, Gerald Jeffrey Snyder, Ian T. Foster, and Anubhav Jain. Matminer: An open source toolkit for materials data mining. 2018.
- [36] Sanford Weisberg. *Applied linear regression*, volume 528. John Wiley & Sons, 2005.
- [37] Dezhen Xue, Deqing Xue, Ruihao Yuan, Yumei Zhou, Prasanna V Balachandran, Xiangdong Ding, Jun Sun, and Turab Lookman. An informatics approach to transformation temperatures of niti-based shape memory alloys. *Acta Materialia*, 125:532–541, 2017.

- [38] Tomoki Yamashita, Nobuya Sato, Hiori Kino, Takashi Miyake, Koji Tsuda, and Tamio Oguchi. Crystal structure prediction accelerated by Bayesian optimization. *Physical Review Materials*, 2:013803, 2018.

## 6 Appendix

### 6.1 Test Case Details

The following are the underlying distributions and function used to generate the synthetic data cases. These test cases were designed to provide a variety of Pareto frontier geometries. For all four synthetic test cases, the output space is two dimensional  $\mathbf{Y} \in \mathbb{R}^2$ , and both outputs are to be maximized.

#### Linear Test Case:

A simple linear frontier geometry, generated by rotating (and stretching) a uniform distribution.

$$\begin{aligned} \mathbf{X}_i &\sim \mathcal{U}[0, 1]^2, \\ \mathbf{Y} &= [X_{i,1} - X_{i,2}, X_{i,1} + X_{i,2}]^\top. \end{aligned} \tag{14}$$

#### Circular Test Case:

A circular frontier geometry, generated via trigonometric functions.

$$\begin{aligned} X_{i,1} &\sim \mathcal{U}[0, 1], \\ X_{i,2} &\sim \mathcal{U}[0, \pi/2], \\ \mathbf{Y}_i &= [X_{i,1} \cos(X_{i,2}), X_{i,1} \sin(X_{i,2})]^\top. \end{aligned} \tag{15}$$

#### Hyperbolic Test Case:

The hyperbolic responses lead to a far greater density of points near the origin. This results in a “sparse” Pareto frontier, which often has very few non-dominated candidates.

$$\begin{aligned} \mathbf{X}_i &\sim \mathcal{U}[0, 10]^2, \\ \mathbf{Y}_i &= [1/X_{i,1}, 1/X_{i,2}]^\top. \end{aligned} \tag{16}$$

#### Bat Test Case:

A non-convex Pareto frontier generated by perturbing the radius of the Circular test-case.

$$\begin{aligned} X_{i,1} &\sim \mathcal{U}[0, 1], \\ X_{i,2} &\sim \mathcal{U}[0, \pi/2], \\ \mathbf{Y}_i &= [(X_{i,1} + 2|X_{i,2} - \pi/4|) \cos(X_{i,2}), (X_{i,1} + 2|X_{i,2} - \pi/4|) \sin(X_{i,2})]^\top. \end{aligned} \tag{17}$$